PNAS
www.pnas.org

**Supplementary Information for**

**A 2020 View of Tension-Based Cortical Morphogenesis**

**David C. Van Essen**
vanessen@wustl.edu

**This PDF file includes:**

Outline of Supplementary Topics, Subtopics, and Figures
Supplementary text Topics 1 - 11
Supplementary Figures S1 to S5
SI References

www.pnas.org/cgi/doi/10.1073/pnas.2016830117

**Outline of Supplementary Topics, Subtopics, and Figures**

*Topic 1. Tension, pressure, and material property measurements.*
*Topic 2. Why does the caudate nucleus have a tail? An explanation, prediction, and confirmation.*
*Topic 3. Why are cerebral and cerebellar cortex thin sheets?*
*Fig. S1. Evidence for passive stretching of the caudate tail during human prenatal development.*
*Fig. S2. Fiber bundle orientation in and near human caudate nucleus revealed by diffusion MRI from the Human Connectome Project (HCP).*
*Topic 4. Cross-sulcal leptomeningeal adherence in cerebral and cerebellar cortex.*
*Fig. S3. Apposed pial surfaces of macaque cerebral cortex.*
*Fig. S4. Apposed pial surfaces of macaque cerebellar cortex.*
*Fig. S5. Large arachnoid spaces in human fetal cerebellum.*
*Topic 5. Cortical folding abnormalities in human brain disorders.*
*Topic 6. The impact of pre-gyrogenesis wiring topology,*
*Topic 7. Individual variability of cortical convolutions and their relationship to cortical areas and connections*
*7a. Folding variability.*
*7b. Area size variability.*
*7c. Folding-function correlations in primate area V1.*
*7d. Connection weight variability.*
*7e. Connectivity and folding perturbations from eye enucleation.*
*7f. Connectivity inferred from diffusion imaging and fMRI.*
*7g. Evaluating folding-connectivity relationships in macaque and human – future prospects.*
*Topic 8. Alternative models of tangential expansion and cortical folding interpreted in the DES+ framework.*
*8a. Radial Intercalation.*
*8b. Differential Proliferation.*
*8c. Differential laminar expansion and cortical buckling.*
*8d. Free Energy.*
*Topic 9. Induced gyrification in model systems – promise and pitfalls.*
*Topic 10. Biomechanical measurements of CNS tissue properties.*
*Topic 11. Extending TBM to other structures.*
*11a. How does the primate retina get its fovea?*
*11b. Hippocampal folding and the unique perforant path.*

***Topic 1. Tension, pressure, and material property measurements.*** It is important to consider whether tension and pressure values observed experimentally in developing neural tissue are in an appropriate range to drive morphogenesis given the observed range of tissue compliance.

*Tension.* Published tension magnitudes are summarized in Fig. 1 and Table 1 in ref. [1]. Neurite tension magnitudes for vertebrate CNS neurons have not to my knowledge been reported. Tension values for neurites and growth cones of vertebrate peripheral neurons *in vitro* range widely, from ~1 – $10^4$ pN. Neurite diameters are not typically measured in such studies, but if one assumes that a neurite typically has a cross-sectional area of ~1 $\mu m^2$, this would correspond to specific tensions ranging from ~1 – $10^4$ Pa ($pN/\mu m^2$). For vertebrate CNS neurons, growth cone and filopodial/lamellopodial tensions are in the

lower end of this range, but they may typically have a smaller cross-sectional area and thus a specific tension in the 10's to hundreds of pascals.

Skeletal muscle provides a useful reference in calibrating and interpreting neurite tension magnitudes. Mammalian fast-twitch skeletal muscles generate force with a specific tension of ~3 kg/cm$^2$ [2] (~300 nN/μm$^2$ = ~3 x 10$^5$ Pa). Thus, the strongest neurites in vitro may generate more than 1% of the specific tension of skeletal muscle. Even the weaker neurites likely generate a specific tension at least 0.001% that of skeletal muscle. If CNS axons, dendrites, and glial processes in vivo generate specific tensions anywhere in this range, this would very likely contribute strongly to morphogenesis, given the high compliance of embryonic CNS tissue noted below.

*Pressure.* During early development of embryonic brain vesicles in the chick, intraluminal pressure is ~15 Pa [3], though much higher estimates have also been claimed [4]. In rats, CSF pressure is 170 – 200 Pa (1.3 – 1.5 mm Hg) in late embryonic development and 330 Pa (2.5mm Hg) from postnatal day y10 onwards [5]. In humans, CSF pressure normally ranges from 200 – 800 Pa (1.5 - 6 mm Hg in term infants, 400 – 930 Pa (3 - 7 mm Hg) in young children, and 1300 – 2000 Pa (10 - 15 mm Hg) in older children and adults [6].

*Tissue stiffness and shear modulus.* In embryonic chicks (Hamburger-Hamilton stages 11-13), Xu et al. [7] used tissue microindentation to measure stiffness values of 0.4 – 1 mdyn/μm, which did not vary systematically across age or region (forebrain, midbrain, hindbrain, or the furrows between them). They used a 3D geometric model to estimate the shear modulus (ratio of shear stress to shear strain, a material property) from indentation stiffness and obtained values of 190 – 280 Pa, again independent of age and region. In the mouse embryonic cortical plate the Young's elastic modulus (ratio of tensile stress to tensile strain) estimated using Atomic Force Microscopy (AFM) ranges from 30 – 110 Pa between ages E12.5 and E18.5, with a peak at E17.5 and modestly higher values in the intermediate and subventricular zones [8]. In rat cortex, the AFM-based Young's modulus is ~450 Pa at p10 and ~1,000 Pa in the adult [9]. In postnatal ferret cortex, microindentation-based stiffness [10] is ~1 mdyn/μm in cortex, subplate, white matter and deep gray matter at P6 and P18, and is ~2 mdyn/μm in these structures in the adult; these correspond to shear moduli estimated to be 40 and 80 Pa, respectively. Altogether, these data suggest that tissue compliance decreases with age (but not always monotonically) and is relatively similar across CNS tissue types for a given age and species. A point to bear in mind is that lipid composition (and hence perhaps mechanical properties) in primate cerebral cortical gray matter varies markedly by age as well as species in a comparison of prefrontal cortex in humans, chimpanzees, and macaques [11].

*Comparison across measures.* To summarize, observed biological pressure differentials during CNS development are commonly in the range of 15 – 800 Pa. Observed shear and elastic moduli in CNS tissue are commonly in the range of 30 – 450 Pa. Observed stiffness values are commonly around 1 mdyn/μm (10nN/μm). Observed neurite tension values are in the range of 1 – 10$^4$ pN, with specific tensions for CNS neurons likely in the range of ~10 – 100 Pa. The wide range of values reported for each of these measures is likely in part to reflect genuine biological variability across regions, species, and developmental age, but experimental error and bias is likely to be a large contributor as well. Continued refinements of existing methods and invention of completely new methods will likely aid in improving these estimates.

To a first approximation, pressure, specific tension, and shear/elastic moduli in CNS tissue appear to be 'in the same ballpark' and are commonly within an order of magnitude of 100 Pa. Stress (such as pressure, Pa) and modulus (Pa) are related by deformation (strain, which is dimensionless). Strain is, roughly, the relative change in a given dimension (e.g., the ratio of change in length to original length), though the relationships are inherently more complex because strain and stress are tensors, materials are nonlinear (modulus changes with deformation), and deformations are 3D (a bar thins as it stretches). When the magnitude of stress approaches the material's modulus, deformations become large; changes in dimension become similar to the original dimensions.

***Topic 2. Why does the caudate nucleus have a tail? An explanation, prediction, and confirmation.*** The main text notes that (i) forebrain subcortical nuclei are populated mainly by neurons having quasi-isotropic dendritic arbors and local axons and (ii) tension in subcortical dendrites and axons can account for why these nuclei generally blob-like (compact) in shape in the adult. Can the isotropic tension hypothesis be reconciled with the fact that some subcortical nuclei have a highly irregular shape? For example, the caudate nucleus in primates has a strikingly long tail that extends posteriorly then curls around and terminates near the amygdala.

A likely explanation comes from considering human caudate development as illustrated in the Bayer & Altman atlases [12-14]. Early in neurogenesis (GW7 – GW9) the striatum (caudate, putamen, and globus pallidus) emerges as a compact, round mass several mm in total extent (Fig. S1A). The internal capsule is prominent from the outset, and its posterior limb separates the putamen from the posterior caudate, which at this early stage lies immediately dorsal to the amygdala. Fig. S1B (GW17) and S1C (GW37) illustrate the progressive expansion of intervening structures (especially thalamus, putamen, globus pallidus, internal capsule, and cerebral peduncles) that collectively push the posterior caudate back, stretching it like taffy into a long tail that extends posteriorly and laterally before looping forward to retain a termination close to the amygdala. This developmental progression suggests that the tail of the caudate arises from passive deformation in response to bulk expansion of neighboring tissue. A prediction is that dendrites and also axons (e.g., cortico-striatal axons and collaterals of intrinsic connections) in the passively stretched tail of the caudate should be elongated along the long axis of the tail, whereas dendrites would remain isotropic in the head of the caudate. One test of this hypothesis would be to evaluate anisotropies in dendritic morphology in the primate tail of the caudate (e.g., using Golgi stains or intracellular injections). However, such analyses have not to my knowledge been reported.

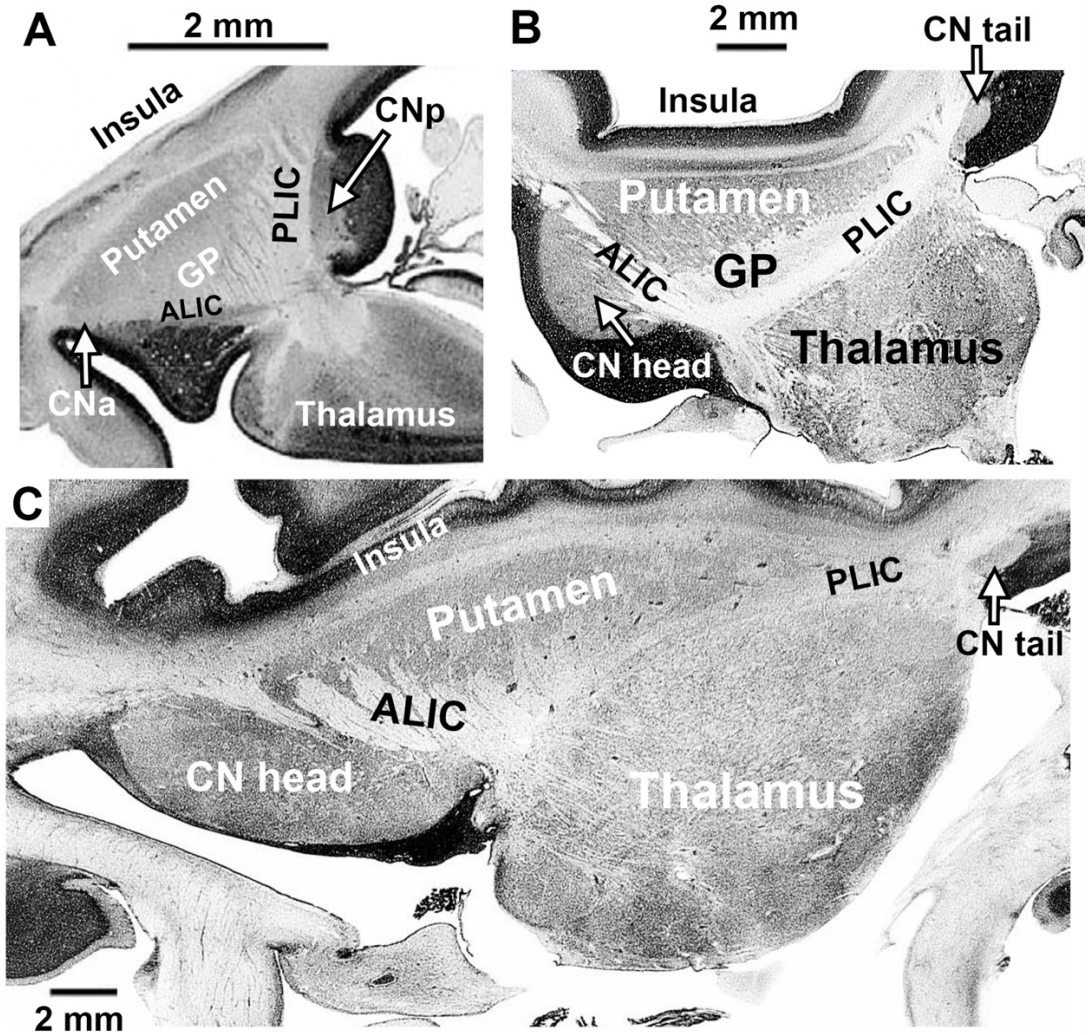


**Fig. S1**. Evidence for passive stretching of the caudate tail during human prenatal development. Quasi-horizontal sections of brains at GW9 (panel A), GW17 (panel B), and GW37 (panel C) [12-14]. A. At GW9 the posterior caudate nucleus (CNp) lies dorsal to the amygdala and is separated from the putamen by the posterior limb of the internal capsule (PLIC), which is already thick at this early stage. The caudate nucleus anterior (CNa) in front of the anterior limb of the internal capsule (ALIC) is smaller than the CNp at this age. B. At GW17 the tail of the caudate (CN tail) is much smaller than the caudate head (CN head) and has shifted posteriorly and laterally. C. At GW37 the size disparity between caudate head and tail is even greater, as is the displacement of the tail posteriorly.

An alternative approach is to use diffusion imaging as an indirect measure of statistical biases in the orientation of elongated cellular elements. To this end, Fig. S2 illustrates neurite orientation anisotropies in the tail of the caudate nucleus in young adults from the Human Connectome Project (HCP). Fig. S2A shows a highly anisotropic antero-posterior orientation bias of fiber bundles (elongated green 'needles' in most voxels) in the left tail of the caudate in one subject, in a region where the tail is thick and runs mainly antero-posteriorly. This is evident in the parasagittal (left panel) and axial (right panel) views; in the coronal view (middle panel) the orientation bias runs orthogonal to

the slice plane and the needles are not visible in most voxels. In a more posterior region (Fig. S2B), an oblique orientation bias is evident in all panels, running parallel to the local long axis of the caudate tail as it shifts laterally, ventrally, and posteriorly in progressing towards its tip. In contrast, in the head of the caudate (Fig. S2C), neurite orientation biases are generally less pronounced (needles shorter or not visible) and more variable in orientation, consistent with the prediction of the TBM model. Similar results were observed bilaterally in four HCP subjects, thus providing strong support for the predicted bias.

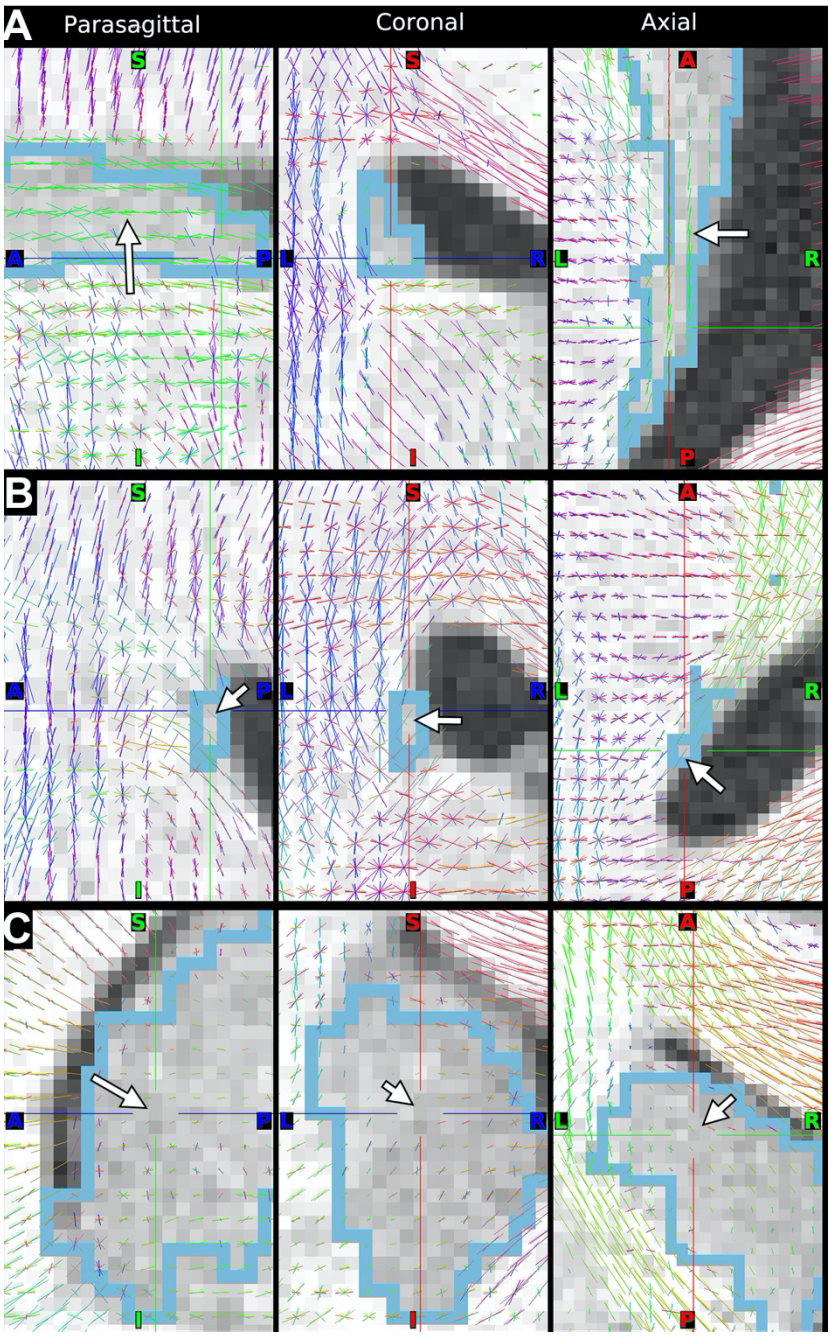


**Fig. S2.** Fiber bundle orientation in and near human caudate nucleus revealed by diffusion MRI from the Human Connectome Project (HCP). Data from exemplar HCP subject 100307 parasagittal (left), coronal (middle) and axial (right) panels from the anterior portion of the caudate tail (row A), a more posterior region (row B), and the head of the caudate (row C). Diffusion imaging scans acquired with 1.25 mm voxel size and other imaging parameters described in ref. [15]. Fiber orientation modeling (up to 3 fiber bundles per voxel) generated using FSL's BedpostX algorithm and other preprocessing steps as described in ref. [15, 16] and displayed using Connectome Workbench visualization software[17]. Fiber bundle length reflects the degree of anisotropy, and the hue indicates bundle orientation (green = A-P bias; red = M-L bias; blue = D-V bias). Fiber orientation data are displayed in native diffusion space and overlaid on structural MRI (T1w scan) at its original 0.7mm voxel size and with FreeSurfer-based automated segmentation of the left caudate nucleus indicated by pale blue outline. Data can be accessed at https://balsa.wustl.edu/study/B432K.

***Topic* 3. *Why are cerebral and cerebellar cortex thin sheets?*** It is interesting to speculate on why, from both evolutionary and computational perspectives, are cerebral and cerebellar cortex thin, laminated sheets that increase dramatically in surface area but not in thickness as a function of brain size. To frame the issues, we first consider two overarching principles that are likely to be important throughout the nervous system.

*3.1 Compact wiring.* Efficient neural computation requires that aggregate wiring length be compact (near-minimal), subject to constraints relating to the biological materials used and the computational algorithms to be executed. A corollary is that computations should be carried out as much as possible using richly interconnected local circuits. Compact wiring is predicted by the general TBM hypothesis and by DES+ Tenet 5; this section explores the implications of this principle.

*3.2 Repetitive and adaptable modular organization.* Once evolution has provided a given lineage with a good architectural design for a patch of sheet-like neural tissue (a module), it can be used repeatedly, but with variations allowed so that replicated modules need not be identical. This may simplify and streamline the developmental instructions needed and also promote evolutionary adaptiveness. This in turn may enable an increasingly diverse range of functions to be mediated by progressive variations on a basic modular scheme.

*3.3 Sheets and layers.* Cerebral cortex, cerebellar cortex, and the retina are prominent sheet-like laminated structures in the CNS of all mammals, with cerebellar cortex and retina present in nearly all vertebrates.

- In each laminar structure, the vast majority of connections are *local but translaminar*, i.e., axons of a neuron in one layer makes most of its synapses locally (typically within ~1-2 mm) but mainly onto dendrites in a different layer [18]. This feature is likely central to how each structure performs its functions. Tension in these radially biased translaminar connections would help keep the layers thin.
- Each laminated sheet has its own distinctive architectural plan and shows different degrees of variation across the sheet.
    - Cerebellar cortex has strikingly uniform cellular architecture across the entire cerebellar sheet in any given species [19, 20], though modest but important spatial nonuniformities do exist [21].
    - The retina has relatively uniform architecture and circuitry across the entire sheet in low-acuity species but has prominent variations in high-acuity species, mainly relating to the fovea and to the systematic decline in retinal ganglion cell density with increasing eccentricity [22].
    - Cerebral neocortex has pronounced variations in architecture across the cortical sheet, as discussed in the next section.

*3.4 Modular organization of cerebral cortex.* Modularity of cerebral neocortex is manifested in two distinct ways: parcellation into distinct cortical areas (parcels) and a finer-grained modularity within individual areas.

- Cerebral neocortex is a mosaic of distinct functional areas, or parcels (~180 per hemisphere in humans [23], ~40 in mice [24], and ~120 - 140 in macaques and marmosets [25].

- Some cortical areas may have arisen through an areal duplication event followed by evolutionary divergence and areal specialization [26, 27].
- The principle of distributed, recursive hierarchical organization allows for many levels of processing, with strongest connectivity between neighboring hierarchical levels [28-30].
- Expansion of neocortex in humans relative to nonhuman primates and also to rodents has occurred preferentially in higher-level association areas of prefrontal, parietal, and temporal cortex [25, 31].
- Architecture varies between neighboring areas, sometimes dramatically but more typically by modest differences. The cumulative regional differences are relatively modest in mice [24]. However, in macaques and humans, regional differences can be dramatic: in higher areas relative to early sensory areas, dendritic arbors are much larger [32], neuronal density is much lower [33], and the degree of myelination is lower [34, 35].

- Within-area modularity is identifiable anatomically in some cortical areas, most clearly in early visual and somatosensory areas.
  - In primate V1, each patch of cortex - a 'hypercolumn' module (~1mm$^2$ surface area in the macaque) analyzes a small region of the visual field, and ~1,000 modules/hemisphere collectively cover the contralateral visual hemifield [36, 37]
  - A coarser modularity occurs in primate area V2 and probably V4, indicating that module size is not identical in all areas [38].
  - In the 'barrel field' of rodent S1, each barrel is dominated by a single vibrissa [39].

*Topic 4. Cross-sulcal leptomeningeal adherence in cerebral and cerebellar cortex.* In countless published human structural MRI images and in many gently processed histological sections from healthy (non-atrophied) adult gyrencephalic brains, opposite banks of cerebral and cerebellar cortical sulci are in immediate apposition along a common boundary at or near the pial surfaces over extended regions, except for gaps where sulcal blood vessels are interposed, as shown for macaque cerebral cortex (Fig. S3) and cerebellar cortex (Fig. S4). The apposition can be very precise in histological sections, suggesting that it reflects physical adhesion rather than simple post-hoc alignment during mounting of tissue sections (see also footnote 17 in ref. [40]. The fact that countless other published images show pronounced gaps between opposite sulcal banks likely reflects two factors: (i) standard tissue processing (sectioning, processing while freely floating, mounting on a slide, solvent immersion, dehydration and tissue staining) leads to substantial tissue shrinkage plus considerable physical stress on each section and (ii) cross-sulcal adhesion is likely weaker than intracortical tissue integrity, making it typically the first to be severed when under physical stress. Also, cortical atrophy during healthy or pathological aging commonly reveals CSF-filled gaps between opposite sulcal banks in structural MRI scans *in vivo*, and this likely involves loss of trans-sulcal adhesions.

To my knowledge there are few if any published analyses of the cellular or molecular basis of adhesion between apposed cortical sulcal banks. An intriguing possibility is that this adhesion might be mechanistically similar to "BM-BM" basement membrane (basal lamina) interactions that are widespread in other tissues and species [41]. The examples they describe of BM-BM interactions commonly involve either sliding or adherence

between BMs from different tissue types. However, in a developing zebrafish dorsal midline fin, a folded epithelial sheet involves adhesion between apposed epithelial BMs mediated by cross-fibers in the ECM that may include hemicentin multimers linked to integrins. The spatio-temporal progression of fin folding (Fig. 3B in ref. [41] is intriguingly similar to the experimentally induced cortical invaginations separated by extended basal lamina ‘fingers’ in human organotypic neocortical slice cultures [42]. These are putatively part of the OCL folding forces hypothesized in DES+ Tenet 3.

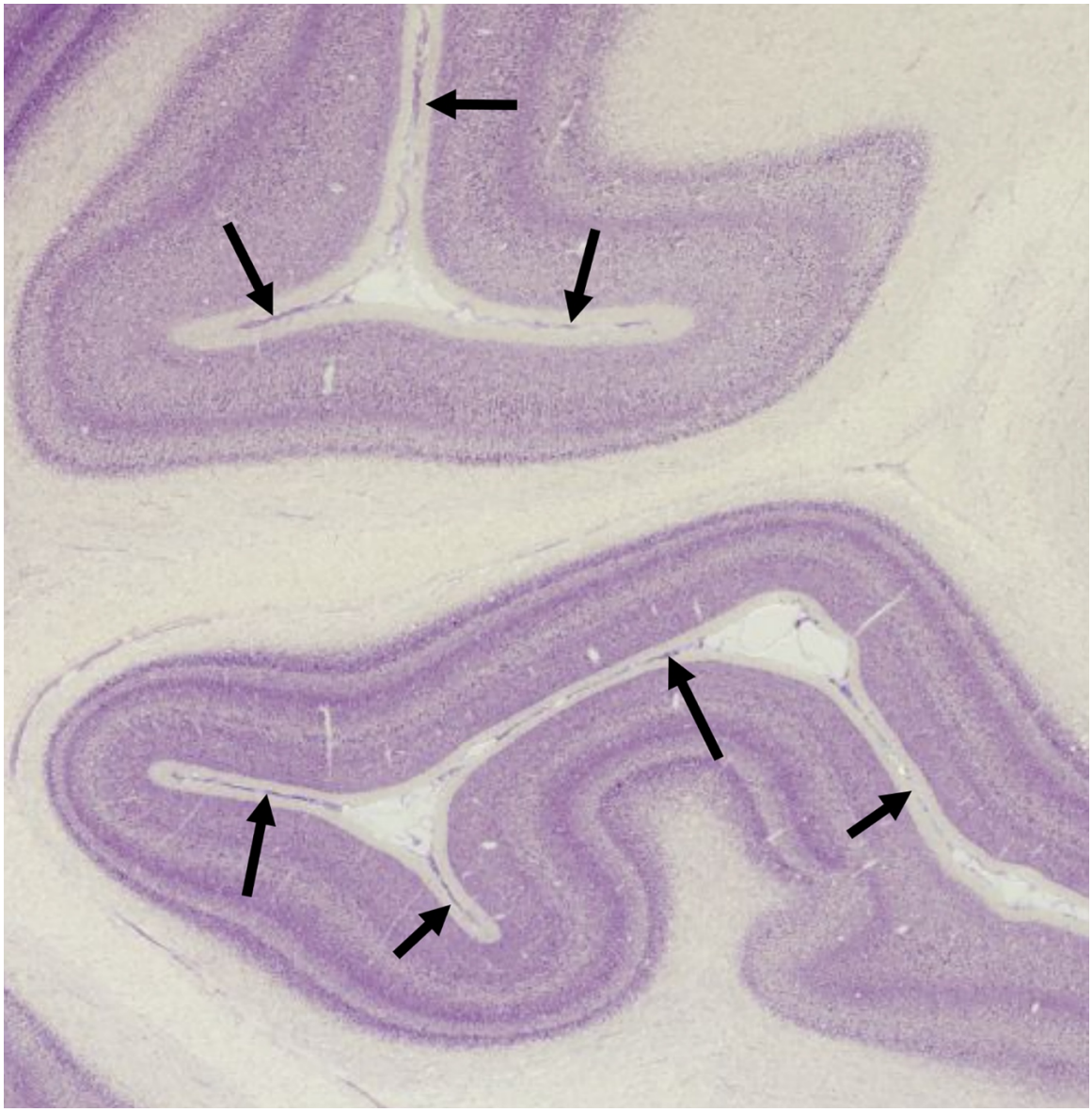

**Fig. S3.** Apposed pial surfaces of macaque cerebral cortex. In gently processed histological sections, apposed banks of sulci generally adhere to one another along a common pia mater margin (arrows), except where blood vessels intervene. Note that there are many published counterexamples of histological sections in which apposed pial surfaces within sulci are partially or completely separated. However, this is in large measure attributable to tissue shrinkage during

histological processing. Image from http://brainmaps.org/ajax-viewer.php?datid=151&sname=0229RH4.z

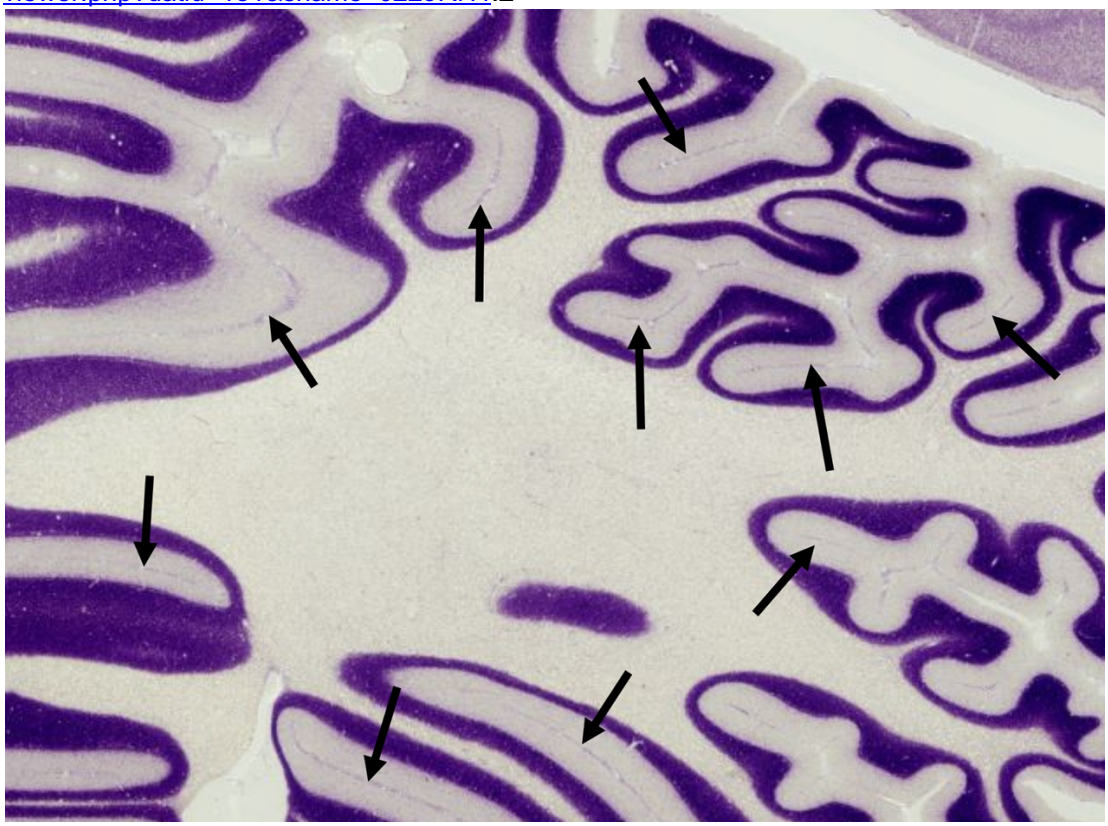

Fig. S4. Apposed pial surfaces of macaque cerebellar cortex. In gently processed Nissl-stained histological sections, apposed banks of cerebellar folds generally adhere to one another along a common pia mater margin, (arrows) except where blood vessels intervene. Note that there are many published counterexamples of histological sections in which apposed pial surfaces within sulci are partially or completely separated. However, this is likely attributable to tissue shrinkage during histological processing. Image from http://brainmaps.org/ajax-viewer.php?datid=151&sname=0380RH4.

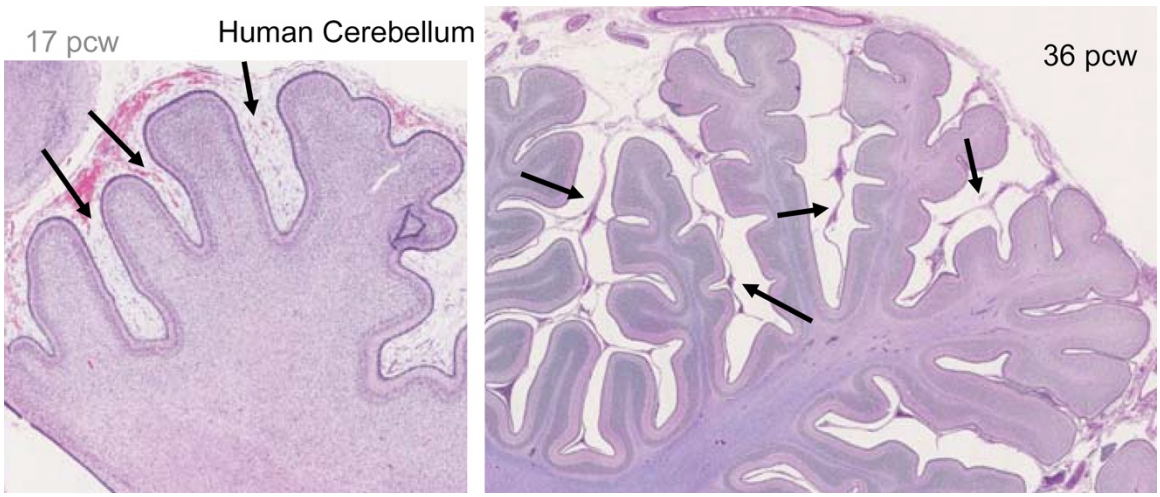


Fig. S5. Large arachnoid spaces in human fetal cerebellum. Large gaps between fetal human cerebellar folds filled with presumed arachnoid tissue (arrows) are evident at 17 postconceptual

weeks (left) and 36 postconceptual weeks (right) in parasagittal sections stained with hematoxylin & eosin. Adapted with permission from ref. [43].

***Topic 5. Cortical folding abnormalities in human brain disorders.*** A wide variety of cortical folding abnormalities have been reported in different brain disorders and in clinical case studies. These provide a valuable testbed for formulating hypotheses for how specific abnormalities might be explained by the DES+ model or other putative mechanisms. Elucidation of the mechanistic underpinnings of particular disorders (e.g., specific gene mutations) might provide evidence on the plausibility of these hypotheses. This section provides a non-exhaustive list of folding abnormalities in cerebral and cerebellar cortex and brief comments on how some cerebral folding abnormalities can be interpreted in the context of the DES+ model.

*Lissencephaly* includes a spectrum of cerebral cortical malformations manifested by abnormally thick cortex (pachygyria) with reduced or absent convolutions (agyria); it is generally associated with abnormal (incomplete) neuronal migration and often also abnormal neuronal proliferation [44, 45]. There are numerous genetic subtypes of lissencephaly, many of which are linked to tubulin-related genetic defects [46]. In many cases, cortical pyramidal neurons lack a tight radial organization [45]. From the perspective of the DES+ model, incomplete migration and abnormal pyramidal cell orientation presumably would both contribute to a reduced radial orientation bias and hence a reduced bias favoring tangential expansion. This in turn can account for increased cortical thickness and reduced gyrification. In other words, the prototypical characteristics of lissencephaly are strongly consistent with predictions from DES+ Tenets 1 (radially biased tension) and 3 (differential tangential expansion).
*Polymicrogyria* typically is expressed as a mixture of ordinary gyri and sulci interspersed with regions having shallower, closely spaced folds that are characterized by deep invaginations of the OCL and smoother undulations of the gray–white border as well as altered lamination, perhaps related to layer-specific degeneration or other pathology especially in deep layers [47]. An early hypothesis attributed the enhanced cortical buckling to exaggerated differential expansion of superficial vs deep layers [40]. However, some microgyria features are reminiscent of many human early cortical sulci (e.g., Fig. 5C,D of main text) as well as the experimentally induced folds in organotypic slice cultures (Fig 2 in ref. [42]). This suggests that polymicrogyria might in part stem from folding involving mechanisms in the OCL layer (DES+ Tenet 3) that are overactive relative to normal development.
Among various other disorders in which cortical folding abnormalities have been reported, Williams Syndrome (WS) is notable for having a spatially distributed set of localized structural abnormalities, several of which show some degree of replicability across studies [48-50] and with many of the abnormalities in regions associated with behavioral characteristics that are distinctive in WS. A more stringent evaluation would be to determine whether WS patients have abnormal patterns of FC that can actually predict specific folding abnormalities such as a shallower olfactory sulcus and a deeper intraparietal sulcus [50].

Several more prevalent brain disorders have been reported to show cortical folding or other structural abnormalities, including autism [51-53], schizophrenia [54], and depression [55, 56]. However, the effects have not in general been as robust as those reported for WS. A possible explanation is that these other disorders are much more diverse and that fractionation into finer-grained subgroups might reveal sub-type specific characteristics.

Cerebellar folding abnormalities are also relatively common in humans and in various mouse mutants [57, 58] but to date have not been studied nearly as intensively as have cerebral folding abnormalities. The mouse is a particularly attractive model for such studies, given its experimental and genetic tractability and the consistency of cerebellar folding in a given mouse strain.

More generally, a promising avenue for the future is to systematically map genetic mutations across patients having brain folding abnormalities. Such mutations may be discovered through exome sequencing studies, and functional experiments elucidating the roles of such genes offer a potentially valuable approach to understanding mechanisms of normal folding

***Topic 6. The impact of pre-gyrogenesis wiring topology***. The establishment of long-distance connections is an extraordinarily complex process in which billions of neurons send axons that must reach their diverse targets by navigating a 3D maze using guidance cues provided by chemotactic gradients and by molecular interactions with scaffolding elements (e.g., radial glial processes) and with neighboring white matter axons. In 2012 Wedeen et al. [59] advanced the provocative 'grid' hypothesis, which proposes that wiring of the brain's white matter is configured in a 3D locally rectilinear grid and that this grid is established by the pathways of the brain following "a base-plan established by the three chemotactic gradients of early embryogenesis". The diffusion MRI analyses underlying this hypothesis have been strongly criticized [60, 61], and an alternative hypothesis has been proposed that brain fiber pathways can be well approximated by a "lamellar vector field"[61].

These competing ideas draw attention to the prospect that topological factors related to crossing fiber bundles may impose major constraints on the compactness of wiring in the adult. As fiber bundles cross one another while establishing long-distance connections during early development, this necessarily forms a highly interlocking meshwork. Whether this mesh conforms to the orderly 'warp and woof' of the Wedeen grid hypothesis, to a completely disordered tangle, or (as seems more probable) to an intermediate quasi-orderly configuration, once a particular intricate topology is established it cannot be changed without severing axons and thus changing connectivity. During gyrogenesis and other large-scale morphogenetic changes, topological constraints may have a dramatic impact on axonal trajectories and the overall compactness of wiring in the adult, as illustrated by the following hypothetical but plausible scenario. Consider two pathways: a long-distance one between widely separated regions 'O' and 'F' (e.g., in occipital and frontal cortex) and a short-distance pathway between two regions that both lie in between O and F (e.g., regions 'P1' and 'P2' in the parietal lobe). Suppose in addition that a gyral fold emerges between P1 and P2, such that they lie on opposite banks of a gyral white matter blade. If the axons that interconnect P1 and P2 are from the outset shallower and completely separate from deeper-running axons that interconnect O and F, then pathway-specific folding may proceed without direct interference between the two pathways. However, if instead there is any intermixing, such that some axons of the local P1-P2 pathway loop under some axons of the O-F pathway, then axonal tension would tend to pull the two sets of interdigitated axons into intermediate trajectories, with the O-F axons pulled partway up into the parietal white matter blade and the P1-P2 axons taking a downward loop en route from one bank to another. Thus, the two hypotheses make very different predictions about the distribution of axonal trajectories in the white matter.

Recent advances in connectomic methods make it feasible to address such questions experimentally. In the lissencephalic mouse, complete reconstructions of the axonal as well as dendritic arborizations of individual neurons reveal their morphology in exquisite detail for a rapidly increasing number of cell reconstructions [62, 63]. Extending such methodology to the gyrencephalic macaque is very challenging, given its 200-fold greater brain size. However, a promising approach has been developed that uses optical clearing of thin brain slabs combined with high-throughput optical scanning, computational alignment between slabs, and semi-automated axonal tracing [64]. Intriguingly, their preliminary observations suggest that the trajectories of some long-distance axons may indeed include loops within a white matter blade that deviate markedly from the most direct route to their target location. If such findings are confirmed and shown to be common rather than outlier cases, it would indicate that aggregate wiring length may be substantially greater than the hypothetical minimal wiring length that would occur if (hypothetically) topology could be rearranged and optimized for adult 3D geometry.

***Topic 7. Individual variability of cortical convolutions and their relationship to cortical areas and connections*.** As noted in the main text, macaques are notable for consistency of cortical folding patterns across individuals (*folding consistency*) and between areal boundaries and folds (*folding-function consistency*). In contrast, humans are notable for a substantial degree of variability in folding from one individual to the next (*folding variability*) and relative to cortical areal boundaries (*folding-function variability*) [65]. This section addresses these issues in more depth based on studies in gyrencephalic species that have already been done or may be feasible in the future. SI Topic 8 below addresses analogous issues for mouse gyrification mutants and for in vitro model systems.

*7a. Folding consistency and variability.* Pathway-specific tension is the only candidate mechanism that can readily account for high folding-function consistency, by virtue of its overt relationship to areal size and connectivity patterns. In contrast, the DES+ model invokes multiple mechanisms that can in principle contribute to folding variability. These include (i) variability in size and/or connection strength profiles of individual cortical areas, both mediated by *pathway-specific tension* (Tenet 2A); (ii) quasi-random variations in the pattern of buckling mediated by *tethering tension* (Tenet 2B) and/or *sulcal invagination* forces in the OCL (Tenet 3); and (iii) variability in the *3D landscape* when the main period of cortical folding commences, based on regional differences in neuronal proliferation and/or migration (Tenet 4).

A general prediction of pathway-specific tension in the context of the DES+ model is that borders between adjacent but weakly connected neighboring areas should tend to run close to sulcal fundi (negative mean curvature) whereas borders between adjacent strongly connected areas should tend to run along gyral crowns. The remaining subsections focus on experimental data and possible future approaches to analyzing variability in cortical area size, connectivity, and the relationships to folds, as this information can provide constraints (but not proof) regarding the relative importance of pathway-specific vs other candidate DES+ mechanisms in accounting for folding-function variability.

*7b. Area size variability.* Each cortical area varies in size (surface area) by two-fold or more across individuals in the two species (macaque and human) that have been

systematically investigated to date. In macaques, these estimates come mainly from studies of visual areas using multiple methods for areal parcellation and are based on modest numbers of animals [66-68]. In humans, size variability estimates come mainly from postmortem cytoarchitectonic analyses of areal volume [69-71] and from a recent in vivo “HCP_MMP1.0” multimodal parcellation of 446 individual HCP subjects using an ‘areal classifier’ applied to cortical surface maps based on cortical myelin and thickness, resting-state functional connectivity (FC), task-fMRI, and visuotopic organization [23].

*7c. Folding-function correlations in primate area V1.* Area V1 is a particularly informative example, as it is the largest cortical area in primates, has by far the most sharply defined architectonic transition along its border with neighboring area V2 (thus minimizing errors in areal delineation in histological sections), and also is associated with the uniquely early-forming calcarine sulcus (Fig. 5 in main text).

In the macaque, the lateral V1/V2 boundary consistently runs close (within 1 – 2 mm) to the gyral folds between the operculum and the lunate sulcus dorsally and the inferior occipital sulcus ventrally; medially, the boundary runs close to the gyral margin along most but not all of the calcarine sulcus [68, 72]. The strong correlation between the V1-V2 boundary and gyral folding is a strong prediction of pathway-specific tension, given that the bi-directional retinotopic pathways linking V1 and V2 are among the most powerful inter-areal pathways in the macaque. (Indeed, on a historical note, this particular relationship was the wellspring for my original 1997 TBM hypothesis.) The fact that the V1/V2 boundary consistently correlates with gyral folds irrespective of its size (surface area) argues that this is not an accidental or coincidental relationship. Another relevant observation is that in many individual macaques, particularly those with larger brains, a small crease (the external calcarine sulcus) occurs roughly in the middle of the operculum, but its presence or absence does not alter the consistent relationship between the V1/V2 border and the deeper folds nearby. This implies that folding variability in one region can coexist with nearby strong correlations between areal boundaries and gyral folds.

In humans, cytoarchitectonic maps of the V1 boundary near the foveal representation at the occipital pole show marked variability relative to local folds [69]. Also, an earlier retinotopic mapping study reported that the vertical meridian along the V1/V2 boundary mainly in the calcarine sulcus is correlated with negative (gyral) mean curvature [73]. The correlation was weaker than that described above for the macaque, though this might in part reflect lower accuracy of mapping the human retinotopic vertical meridian. More accurate estimates of the human V1 boundary are now available in two independent HCP datasets: the aforementioned HCP_MMP1.0 parcellation based on 3T data that includes the full extent of V1 and a higher resolution human 7T retinotopy dataset for the central visual field representation from 183 HCP subjects [74]. A systematic comparison of folding vs V1 boundaries is feasible and would be of general interest. But there is little doubt about the qualitative conclusion that folding-function correlations are significant but also more variable in human than macaque V1/V2. An important corollary question is whether the gyral folds along the margins of the early-forming CaS occur close to the V1/V2 boundary even though they may precede the establishment of connections between V1 and V2. It is plausible that this fold gradually shifts during development relative to the architectonically well-defined V1/V2 border.

*7d. Connection weight variability.* In the two species that have been systematically investigated to date using quantitative anatomical retrograde tracer data, the connection

weight between a given pair of cortical areas (expressed as a “Fraction of Labeled Neurons” – FLN) varies across individuals by about one order of magnitude or less in both the mouse [24]; see also [75] and macaque [30, 76]. This within-pathway variability is a small fraction of the five orders of magnitude range in average connection strength across all pathways analyzed in these species.

7e. *Connectivity and folding perturbations from eye enucleation.* Experimental perturbations that affect cortical parcellation and/or connectivity offer potential for systematically exploring the relationship between connectivity and folding. For example, prenatal binocular eye enucleation in the macaque dramatically affects cortical architecture, parcellation, folding, and connectivity [77-80]. The size of area V1 is markedly reduced; islands and patches of nonstriate cortex known as ‘area X’ [80], and ‘default extrastriate cortex (DEC)’ [78], or ‘hybrid cortex (HC)’ [79] occur within or adjacent to V1. The boundary of V1 is often far from the gyral margins of the lunate and inferior occipital sulci, and additional dimples or wrinkling of opercular cortex are common. An important issue is whether these altered folding-vs-function relationships are related to altered connectivity between V1 and adjacent regions that might impact pathway-specific tension (DES+ Tenet 2A). The existing data on connectivity patterns after enucleation are insufficient to resolve this issue [79]. Another observation is that prenatal enucleation causes a dramatic loss of LGN neurons [77]. Hence, enucleation effects are not simply attributable to silencing of retinal activity but may in addition reflect changes in trophic interactions normally mediated by thalamocortical circuitry. Thus, while the effects of enucleation on cortical folding are intriguing, it is difficult to make strong inferences about the mechanistic underpinnings based on current knowledge.

7f. *Connectivity inferred from diffusion imaging and fMRI.* Connection weights can also be assessed using tractography based on diffusion imaging (dMRI) and by FC based on rfMRI, but both measures are very indirect. Tractography is conceptually a more direct approach, insofar as it uses fiber bundle orientations and trajectories within the white matter to estimate the anatomical pathways linking different gray matter regions. Unfortunately, this approach is highly susceptible to errors and systematic bias, including a major ‘gyral bias’ related to cortical folding patterns that impacts sulcal fundi more severely than gyral crowns [81-83]. Hence, current state-of-the-art dMRI and tractography is not well suited for rigorous quantification of individual variability in anatomical connectivity.

FC from resting-state fMRI can be based on the correlation of BOLD signal fluctuations between pairs of grayordinates (surface vertices plus subcortical gray matter voxels), parcels, or other ROIs. These correlations are likely influenced by indirect as well as direct anatomical connectivity between the selected ROIs as well as by common inputs [84, 85]. Analysis strategies such as using partial correlation instead of full correlation might in principle provide better estimates of direct connectivity, but preliminary efforts along these lines suggests that the relationships are more complex [86]. Biases related to cortical geometry and folding are another concern, as it may include partial volume effects as well as sensitivity to venous signals that reflect drainage from opposing banks of a sulcus. Nonetheless, FC analyses may be less severely impacted by folding-related biases than is tractography and hence are more promising as a semi-quantitative approach to estimating anatomical connectivity (see topic 7g below).

7g. *Evaluating folding-connectivity relationships in macaque and human – future prospects.* The previously noted prediction that sulcal fundi should tend to separate

weakly connected regions, whereas gyral crowns should tend to separate strongly connected neighboring regions is amenable to systematic evaluation, using neuroanatomical tracers in animal models, particularly the macaque, and using neuroimaging methods in humans and macaques.

To analyze folding-connectivity correlations using anatomical tracers, it is highly desirable to have quantitative, 'parcellation-free' analyses of 'dense' tracer-based connectivity accurately mapped to cortical surface models. This has only rarely been achieved in the past (e.g., ref. [87], largely owing to challenges in obtaining accurate surface models of the hemispheres that were injected and analyzed histologically. A promising alternative is to align histological sections to an MRI-based atlas surface model using a novel 'contours-to-surface' method [86], taking advantage of the consistency of folding patterns across individual macaques.

To address analyze folding-connectivity correlations using analyses of FC from fMRI, a prerequisite is to have large amounts of high quality and high spatial resolution fMRI data mapped to the cortical surface. Such datasets are available in the YA-HCP 3T and 7T datasets described above and are becoming available in the macaque as well [86, 88].

Another consideration is that novel advances in light microscopic methods may open exciting new opportunities for analyzing long-distance connectivity in gyrencephalic brains without the use of anatomical tracers. For example, novel imaging systems can leverage polarized light properties to infer fiber orientations in postmortem human brains [89, 90]

***Topic 8. Alternative models of tangential expansion and cortical folding interpreted in the DES+ framework.*** This section evaluates four published models of cortical expansion and folding.

*8a*. *Radial Intercalation*. The Radial Intercalation model [91] for preferential tangential expansion proposes that newly migrated neuronal cell bodies intercalate between existing neurons within the cortical plate and that "the translocating cell body pushes the neighboring cell bodies tangentially aside". As noted in relation to Fig. 1 in the main text, the direction of migration is irrelevant to the axis of preferential expansion. Indeed, to explain why cells are pushed tangentially rather than radially, the authors further stipulate that the "outer cortical plate is bonded to the deeper layers of the cortical plate (through radial processes and intercellular adhesion)". This is tantamount to invoking radially biased tension, is consistent with DES+ Tenet 1, and arguably does not constitute a separate, distinct mechanism.

*8b. Differential Proliferation.* Another model invokes differential proliferation underneath gyral vs sulcal regions leading to *tangential dispersion* of neurons in presumptive gyral regions as explanations for both preferential tangential expansion and cortical folding [92-94]. Differential proliferation is indeed important in generating the 3D geometrical landscape prior to the onset of cortical folding, as noted in Fig. 4 of the main text and in DES+ Tenet 4. However, differential proliferation *per se* does not specify what morphogenetic forces actually shape the cortex. The tangential dispersion model describes 'splaying out' of migration trajectories in a nascent gyral bulge over a region of elevated proliferation. However, whether migrating neurons stack up to make cortex locally thicker or diverge to keep cortex thin and increase surface area depends not on

proliferation but on forces within the CGM and principles of tissue expansion such as those illustrated in Fig. 1 of the main text. By DES+ Tenet 1, tangential dispersion is a consequence, not a cause of tangential expansion.

*8c. Differential laminar expansion and cortical buckling.* An early DTE model of Richman et al. [40] proposed that "differential growth between the outer and inner portions of the cerebral cortex" causes cortical buckling (and that the extreme folding observed in polymicrogyria reflects excessive buckling – see SI Topic 5). Their evidence for normal differential growth is based on finding ~10% greater surface area in superficial vs deep layers in the normal hemisphere of one GW27 brain that had microgyria in the opposite hemisphere. Their buckling model invoked differential growth of superficial vs deep cortical layers surrounding a slower-growing white matter core of much lower stiffness. They identified parameter ranges in which buckling occurred with a 'wavelength' ~8-fold greater than cortical thickness and comparable to that in human cortex. However, consistency with a few anatomical observations does not constitute strong support for the model. As noted in the main text, the gel-brain simulation model [95] achieves a much better fit to observed human convolutions based on differential tangential expansion between a uniform cortical sheet and an underlying core having roughly similar elastic moduli. Also, the evidence for greater surface area of superficial vs deep layers is attributable to gyri in general being thicker than sulci, particularly in superficial layers, which in turn is arguably a consequence rather than a cause of cortical folding [96].

*8d. Free Energy.* The Mota and Herculano-Houzel Free Energy model of cortical folding [97] represents a very different mechanistic analysis. It starts with the striking empirical observation that total cortical surface area (AG), exposed cortical surface area (AE), and cortical thickness (T) conform tightly to a relationship in which the product of AG and $T^{0.5}$ ($AG * T^{0.5}$) is proportional to $AE^{\sim 1.3}$ across a wide range of mammals. Moreover, a similar relationship holds for crumpled paper sheets - another fractal self-avoiding surface.

In order to link these empirical observations to the development of cortical folds, the authors (in their supplementary material section) formulate a free energy model that aims to "incorporate the known mechanics and organization of elongating axonal fibers". They derive from their model a prediction that $AG * T^{0.5}$ is proportional to $AE^{\sim 1.25}$, i.e., similar to the empirically determined exponent. This leads them to propose that development effectively follows a free energy gradient until reaching a minimum that also corresponds to a minimum aggregate wiring length, subject to other constraints. They conclude that "Folding is therefore an intrinsic, fractal property of a self-avoiding surface, whether biological or not, subjected to crumpling forces that depends simply on the relative lateral expansion of this sheet relative to its thickness, regardless of how densely neurons are distributed within it."

While the free energy model is both clever and intriguing, it also makes multiple questionable assumptions and obvious oversimplifications, and it is additionally inconsistent with a number of experimental observations. One debatable assumption is that the 'equilibrium' length of each axon can be adequately expressed by minimizing a potential energy containing only two terms, one related to axonal tension and the other related to 'external forces'. Given the complex configuration of 'external forces' on individual axons, the axonal energy landscape might commonly have a complex profile that leads to local minima far from a global minimum. Another assumption is that the 'volumetric energy' for the cortex can be adequately expressed by a linear equation

proportional to total white matter volume and to CSF pressure. This seems problematic insofar as the pressure gradient declines within the brain parenchyma by an unknown but likely complex spatial pattern. A third assumption, that 'surface energy' associated with the shape of the cortical surface can be adequately expressed by a self-avoidance term plus "whatever other surface energy terms one cares to include", is inherently weak owing to the vagueness of the last phrase. A fourth assumption is that connectivity patterns within the white matter naturally segregate into deep long-distance connections that preferentially interconnect deep portions of sulci and shallow shorter-range connections that preferentially interconnect regions within gyri. However, no evidence is presented that cortical connectivity conforms to such predictions, particularly for their specific and highly constrained geometric formulation (see also SI Topic 6). A final example is their assumption that "All sulci and gyri originally form at the same scale, but the surface expansion means that earlier forming structures will become larger and deeper and will connect more distant regions, and that the larger structures will themselves be composed of smaller ones iteratively, down to the minimal, fundamental scale at which they are originally formed. This structure of nested self-similar structures precisely characterizes a fractal object." This assumption is inconsistent with the observed pattern of early sulcus formation in humans (Fig. 5 of main text) and with other characteristics of gyrification evident in refs [12-14]. Altogether, the free energy model appears to be highly speculative, and the observed similarity of the power law exponent to that derived empirically by a totally different approach may be largely coincidental.

***Topic 9. Induced gyrification in model systems – promise and pitfalls***. As noted in the main text, there are several promising model systems for mechanistic studies of cortical gyrification. These include induced gyrification in mice and in human organotypic slice cultures and stem-cell-derived cerebral organoids, and perturbation of gyrification in ferrets. There are also important issues to consider regarding what constitutes gyrification and how best to explore the underlying mechanisms while avoiding pitfalls. Particularly attractive are systems that induce robust and consistent folding that emulates either the full set of folding characteristics or selected characteristics that enable focusing on a subset of mechanisms involved. Also relevant is whether the method used to induce folding taps into signaling mechanisms plausibly involved in normal gyrogenesis or instead represents an 'unnatural' perturbation that achieves a similar outcome.

The patterns of tissue folding reported in different studies are diverse, but most fall into two broad categories identified as 'bona fide cortical folding' and 'pseudo cortical folding' by Borrell [98]. Bona fide cortical folding, as occurs in normal neocortex of all gyrencephalic species, involves a cortical ribbon that is folded along both the pial and gray/white boundary, so that the underlying white matter (or cortical subplate) has 'blades' that separate opposing sulcal banks; the ventricular surface, in contrast, is generally smooth. Pseudo cortical folding generally involves wrinkling or buckling of the entire cerebral sheet, including both pial and ventricular surfaces; it typically involves a neuroepithelial sheet that has not differentiated into a cortical plate distinct from the germinal layer(s). In general, pseudo folding differs so profoundly from bona fide folding that it is arguably of limited utility for exploring the mechanisms of normal gyrification.

Among the more promising mouse gyrification mutants are ones involving expression of the hominoid-specific gene TBC1D3 via electroporation or transgenesis [99] or from electroporation-based knockdown of the DNA-associated protein Tmp1 [100]. These cause a single invagination analogous to the dimples reported here in early human

cortex (Fig. 5B, C in main text). Other examples include transgenic knockout deletions of adhesion molecules FLRT1 and FLRT3 in mice that lead to multiple shallow and occasionally deeper sulci [101], electroporation-induced expression of the human-specific and radial glia-specific gene ARHGAP11B that induces modest superficial invaginations, and selected Foxc1 transgenic hypomorphs that can cause notably complex undulations (see Fig. 1C in ref. [102]). Interestingly, intraventricular injection of FGF2 protein causes a crease-like invagination mainly involving superficial layers, with only a slight inward curving of the gray-white border [103]. This is suggestive of effects that might be concentrated in the OCL zone (DES+ Tenet 3). The FGF family is also of particular interest in view of perturbation experiments in ferrets that implicate FGF in regulation of cortical folding [104, 105].

Apoptosis is not known to have a major role in normal gyrogenesis, but it is nonetheless noteworthy that another class of mouse gyrification mutants involves increase in neuronal numbers via inhibition of apoptosis. Patterns suggestive of bona fide folding have been reported for some caspase knockouts [106] and from perturbation of ephrin signalling by EphA7 knockout [107]. Other caspase knockouts produce expanded cortex with amorphous blobs but a lack of convincing sulci or gyri [108, 109]. Finally, examples of pseudo folding include beta-catenin overexpressing mice [110] and lysophosphatidic-acid-treated embryonic explants [111].

There is understandable interest in using human stem-cell-derived cerebral organoids as a model system for various aspects of cortical development. However, to date, only pseudo cortical folding has been demonstrated in cerebral organoids [112, 113]. In contrast, in vitro human organotypic slice cultures and free-floating cortical tissue culture have already proven to be a promising approach for experimental analyses of the mechanisms of cortical folding [42]; see also main text and SI Topic 4.

***Topic 10. Biomechanical measurements of CNS tissue properties.*** The DES+ and CMS models predict specific patterns of anisotropic tissue compliance in different compartments of cerebral and cerebellar cortex and underlying white matter. These features in principle should be detectable and quantifiable using appropriate biomechanical methods. One promising approach is MR elastography (MRE) combined with focused ultrasound. MRE is based on encoding of harmonic displacement by oscillating magnetic field gradients (“motion encoding gradients”) that are inserted between the imaging gradients of a spin-echo MR imaging pulse sequence, analogous to diffusion encoding gradients used in dMRI [114]. Conventional MRE for in vivo studies typically generates oscillating tissue displacements using a vibrating “actuator” that is coupled to the skull in a fixed configuration. This does not allow systematic control over the axis of vibration and hence is not well suited for mapping anisotropic tissue properties at different locations. A promising recent development involves the use of focused ultrasound (FUS) rather than a physical actuator to induce systematically controllable tissue vibration patterns [115, 116]. Another involves multi-excitation MRE based on two orthogonally placed vibrators [117]. If these or other methods can be further refined so as to achieve sufficient spatial resolution (sub-cm) and sensitivity in vivo in humans or in animal models (e.g., macaque or ferret), they might be able to assess whether cerebral white matter regions dominated by a primary fiber orientation (as assessed using diffusion imaging) show a corresponding anisotropic compliance. For cerebellar cortex a primary question of interest is whether the molecular layer (ML) is stiffer along the axis of folding (parallel to the parallel fibers) compared to the transverse axis. Given the collinearity of the ‘accordion-like’ cerebellar folds over large expanses,

this anisotropy may be manifested over a larger spatial scale than individual folia and thus addressable using FUS-MRE.

***Topic 11. Extending TBM to other structures****.* My original TBM paper [118] focused on cerebral neocortex and cerebellar cortex, as does the current study, but it also proposed specific tension-based mechanisms that could account for key aspects of morphogenesis in two other structures: the foveal pit of the primate retina and the curled configuration of the hippocampal cortex. Here, I briefly review recent evidence bearing on these hypotheses.

*11a. How does the primate retina get its fovea?* In humans and many other primates, the fovea provides for maximal visual acuity in the center of gaze by virtue of (i) a very high cone density and (ii) a foveal pit that allows for maximum image quality by way of centrifugal displacement of cell layers interior to the photoreceptor layer [22, 119]. As a result, cones in the foveal center (foveola) have long photoreceptor axons (fibers of Henle) that link to displaced retinal ganglion cells (RGCs) by way of interposed (and displaced) bipolar and other cells in the inner nuclear layer (INL). A key early developmental event is that RGCs in the area centralis (the foveal precursor) appear to send axons that radiate centripetally; axons initially directed temporally (away from the optic disk) take a curved trajectory as needed to exit the retina at the optic disk in the nasal retina [120, 121]; see Fig. 4 in [119].

As part of the general TBM hypothesis [118], I proposed a foveal 'axonal anchoring' model involving tension along a multicellular link between RGC axons anchored at one end in the inner nerve fiber layer (subjacent to the inner limiting membrane and before axonal trajectories begin to curve) and at the other end in the outer limiting membrane where photoreceptor axons join photoreceptor cell bodies. Because the anchoring points for the RGC axons are displaced from the cone cell bodies, tension would displace the intervening cellular components. If photoreceptor axons are the most compliant, they would be stretched the farthest, becoming fibers of Henle, and the other components in the inner nuclear and plexiform layers would be displaced the most and remain in approximate radial alignment with one another, as also occurs for the intercalated Muller glial cells that extend between inner and outer limiting membranes (cf. Fig. 13 in [119]).

Springer et al. [122] raised several criticisms of the axonal anchoring model ('axonal towing' in their terms). One is the assertion that because RGC axons have exited the retina long before foveal displacement occurs, axonal tension would be unable to exert its proposed effect. However, this criticism is flawed because axonal tension can mediate cellular displacement at any time, not just when axonal outgrowth is occurring. Another is that because nuclear layers are likely to be stiffer than axonal layers, RGC axons would be unable to displace (tow) the RGC cell bodies, let alone bipolar cells. However, if many neighboring RGC axons are pulling in concert, they should be able to displace a 'raft' of RGC cell bodies. A third criticism is that axonal anchoring "does not address how inner nuclear layer neurons are displaced laterally". However, this issue was explicitly addressed previously [118] and is restated above.

Several other mechanisms have been proposed to contribute to foveal displacement: (i) enhanced elasticity of the inner retinal layers in the avascular and astrocyte-free central part of the fovea (foveola), coupled with intraocular pressure [122, 123]; (ii) tangential stretching of retinal tissue due to eye growth [124, 125]; and (iii) horizontal contraction of Muller cell side processes [119]. Altogether, the axonal anchoring model remains a

plausible and attractive hypothesis for centripetal displacement events in foveal pit development, and I am not aware of any strong evidence against it. However, other mechanisms may be involved as well. To test these hypotheses, laser photoablation experiments of the type espoused in the main text are a particularly attractive approach because excellent access can be obtained in retinal whole mount preparations without tissue slicing. Specific predictions are that severing foveal RGC axons near the soma should result in retraction, as should severing of photoreceptor fibers of Henle. Another important and tractable but understudied issue is the mechanism that induces centrifugal outgrowth of RGC axons. Might this be a diffusible morphogen that repels axonal growth cones and has its highest concentration in the area centralis?

The axonal anchoring model does not account for the dramatic (10-fold or more) increase in foveal cone density, which occurs over an extended period (both prenatally and postnatally in humans) and is associated with a reduction in diameter and corresponding elongation of cones [119]. The mechanism of these cone shape changes remain unclear but may include intrinsic shape changes mediated by FGF signaling [126-128], molecular interactions that affect membrane curvature [129] and/or mechanical interactions with Muller cells [119].

*11b. Hippocampal folding and the unique perforant path.* The perimeter of the cerebral cortical sheet includes several distinctive structures, one of which is the hippocampal complex. Hippocampal cortex is separated from neocortex by intervening strips of transitional cortex, including entorhinal cortex (adjoining neocortex) and the subicular complex (between entorhinal cortex and hippocampal subfields CA1-4). The pyramidal cell layer of CA4 terminates abruptly and is capped by the tooth-like dentate gyrus (DG). A striking feature is that the hippocampus is sharply creased, so that the dentate gyrus folded is directly apposed to the subicular complex. This is important functionally because the perforant path (PP) is a major anatomical pathway that links entorhinal cortex (ER) to the DG [130]. It is unique because it is the only pathway known whose axons traverse apposed pial surfaces. For example, in early postnatal rats, axons from superficial ER layers cross the underlying white matter, the full thickness of subicular cortex, and the subicular-DG gap to invade the DG molecular layer [131, 132].

In the original TBM study [118] I proposed that mechanical tension along axons of the PP are under tension and help ensure that the two regions remain in close proximity. This remains a plausible hypothesis, and to my knowledge there is no direct evidence against the model. However, the aforementioned evidence for cross-sulcal leptomeningeal adherence (DES+ Tenet 3 and SI Topic 4) as a general mechanism for adherence of apposed sulcal banks could plausibly be involved as well. Once again, the photoablation method could provide an attractive experimental approach, as it might reveal whether PP axons are under tension as they cross the subicular-DG gap.

## SI References


1. Athamneh, A.I. and D.M. Suter, *Quantifying mechanical force in axonal growth and guidance.* Front Cell Neurosci, 2015. **9**: p. 359.
2. Burke, R.E., *Motor units: Anatomy, physiology and functional organization.* , in *Handbook of Physiology, Section 1: The Nervous System.* , V.B. Brooks, Editor. 1981, American Physiological Society: Bethesda MD. p. 345-422.
3. Garcia, K.E., et al., *Molecular and mechanical signals determine morphogenesis of the cerebral hemispheres in the chicken embryo.* Development, 2019. **146**(20).

4. Desmond, M.E., M.L. Levitan, and A.R. Haas, *Internal luminal pressure during early chick embryonic brain growth: descriptive and empirical observations.* Anat Rec A Discov Mol Cell Evol Biol, 2005. **285**(2): p. 737-47.
5. Jones, H.C., R. Deane, and R.M. Bucknall, *Developmental changes in cerebrospinal fluid pressure and resistance to absorption in rats.* Brain Res, 1987. **430**(1): p. 23-30.
6. Rangel-Castilla, L., S. Gopinath, and C.S. Robertson, *Management of intracranial hypertension.* Neurol Clin, 2008. **26**(2): p. 521-41, x.
7. Xu, G., et al., *Opening angles and material properties of the early embryonic chick brain.* J Biomech Eng, 2010. **132**(1): p. 011005.
8. Iwashita, M., et al., *Systematic profiling of spatiotemporal tissue and cellular stiffness in the developing brain.* Development, 2014. **141**(19): p. 3793-8.
9. Elkin, B.S., A. Ilankovan, and B. Morrison, 3rd, *Age-dependent regional mechanical properties of the rat hippocampus and cortex.* J Biomech Eng, 2010. **132**(1): p. 011010.
10. Xu, G., et al., *Axons pull on the brain, but tension does not drive cortical folding.* J Biomech Eng, 2010. **132**(7): p. 071013.
11. Li, Q., et al., *Changes in Lipidome Composition during Brain Development in Humans, Chimpanzees, and Macaque Monkeys.* Mol Biol Evol, 2017. **34**(5): p. 1155-1166.
12. Bayer, S.A.a.A.J., *The Human Brain During the Late First Trimester*. Atlas of Human Central Nervous System Development. 2006: CRC Press.
13. Bayer, S.A.a.A.J., *The Human Brain During the Second Trimester*. Atlas of Human Central Nervous System Development. 2005: CRC Press.
14. Bayer, S.A.a.A.J., *The Human Brain During the Third Trimester* Atlas of Human Central Nervous System Development. 2003: CRC Press.
15. Sotiropoulos, S.N., et al., *Advances in diffusion MRI acquisition and processing in the Human Connectome Project.* Neuroimage, 2013. **80**: p. 125-43.
16. Glasser, M.F., et al., *The minimal preprocessing pipelines for the Human Connectome Project.* Neuroimage, 2013. **80**: p. 105-24.
17. Hodge, M.R., et al., *ConnectomeDB--Sharing human brain connectivity data.* Neuroimage, 2016. **124**(Pt B): p. 1102-1107.
18. Callaway, E.M., *Local circuits in primary visual cortex of the macaque monkey.* Annu Rev Neurosci, 1998. **21**: p. 47-74.
19. Eccles, J.C., Ito,M., and Szentagothai, J., *The Cerebellum as a Neural Machine*. 1967, Berlin, Heidelberg, New York: Springer-Verlag.
20. D'Angelo, E. and S. Casali, *Seeking a unified framework for cerebellar function and dysfunction: from circuit operations to cognition.* Front Neural Circuits, 2012. **6**: p. 116.
21. Cerminara, N.L., et al., *Redefining the cerebellar cortex as an assembly of non-uniform Purkinje cell microcircuits.* Nat Rev Neurosci, 2015. **16**(2): p. 79-93.
22. Hoon, M., et al., *Functional architecture of the retina: development and disease.* Prog Retin Eye Res, 2014. **42**: p. 44-84.
23. Glasser, M.F., et al., *A multi-modal parcellation of human cerebral cortex.* Nature, 2016. **536**(7615): p. 171-178.
24. Gamanut, R., et al., *The Mouse Cortical Connectome, Characterized by an Ultra-Dense Cortical Graph, Maintains Specificity by Distinct Connectivity Profiles.* Neuron, 2018. **97**(3): p. 698-715 e10.
25. Van Essen, D.C. and M.F. Glasser, *Parcellating Cerebral Cortex: How Invasive Animal Studies Inform Noninvasive Mapmaking in Humans.* Neuron, 2018. **99**(4): p. 640-663.
26. Grove, E.A. and T. Fukuchi-Shimogori, *Generating the cerebral cortical area map.* Annu Rev Neurosci, 2003. **26**: p. 355-80.
27. Chakraborty, M. and E.D. Jarvis, *Brain evolution by brain pathway duplication.* Philos Trans R Soc Lond B Biol Sci, 2015. **370**(1684).
28. Maunsell, J.H. and D.C. van Essen, *The connections of the middle temporal visual area (MT) and their relationship to a cortical hierarchy in the macaque monkey.* J Neurosci, 1983. **3**(12): p. 2563-86.
29. Felleman, D.J. and D.C. Van Essen, *Distributed hierarchical processing in the primate cerebral cortex.* Cereb Cortex, 1991. **1**(1): p. 1-47.

30. Markov, N.T., et al., *A weighted and directed interareal connectivity matrix for macaque cerebral cortex.* Cereb Cortex, 2014. **24**(1): p. 17-36.
31. Donahue, C.J., et al., *Quantitative assessment of prefrontal cortex in humans relative to nonhuman primates.* Proc Natl Acad Sci U S A, 2018. **115**(22): p. E5183-E5192.
32. Elston, G.N., *Cortex, cognition and the cell: new insights into the pyramidal neuron and prefrontal function.* Cereb Cortex, 2003. **13**(11): p. 1124-38.
33. Collins, C.E., et al., *Neuron densities vary across and within cortical areas in primates.* Proc Natl Acad Sci U S A, 2010. **107**(36): p. 15927-32.
34. Glasser, M.F., et al., *Trends and properties of human cerebral cortex: correlations with cortical myelin content.* Neuroimage, 2014. **93 Pt 2**: p. 165-75.
35. Glasser, M.F. and D.C. Van Essen, *Mapping human cortical areas in vivo based on myelin content as revealed by T1- and T2-weighted MRI.* J Neurosci, 2011. **31**(32): p. 11597-616.
36. Hubel, D.H. and T.N. Wiesel, *Uniformity of monkey striate cortex: a parallel relationship between field size, scatter, and magnification factor.* J Comp Neurol, 1974. **158**(3): p. 295-305.
37. Van Essen, D.C.a.A., C.H., *Information processing strategies and pathways in the primate retina and visual cortex.*, in *Introduction to Neural and Electronic Networks*, S.F. Zornetzer, Davis, J.L., Lau, C. , Editor. 1990, Academic Press: Orlando FL. p. 43-72.
38. DeYoe, E.A., et al., *Multiple processing streams in occipitotemporal visual cortex.* Nature, 1994. **371**(6493): p. 151-4.
39. Petersen, C.C., *The functional organization of the barrel cortex.* Neuron, 2007. **56**(2): p. 339-55.
40. Richman, D.P., et al., *Mechanical model of brain convolutional development.* Science, 1975. **189**(4196): p. 18-21.
41. Keeley, D.P. and D.R. Sherwood, *Tissue linkage through adjoining basement membranes: The long and the short term of it.* Matrix Biol, 2019. **75-76**: p. 58-71.
42. Long, K.R., et al., *Extracellular Matrix Components HAPLN1, Lumican, and Collagen I Cause Hyaluronic Acid-Dependent Folding of the Developing Human Neocortex.* Neuron, 2018. **99**(4): p. 702-719 e6.
43. Haldipur, P., et al., *Spatiotemporal expansion of primary progenitor zones in the developing human cerebellum.* Science, 2019. **366**(6464): p. 454-460.
44. Di Donato, N., et al., *Analysis of 17 genes detects mutations in 81% of 811 patients with lissencephaly.* Genet Med, 2018. **20**(11): p. 1354-1364.
45. Friocourt, G., et al., *Role of cytoskeletal abnormalities in the neuropathology and pathophysiology of type I lissencephaly.* Acta Neuropathol, 2011. **121**(2): p. 149-70.
46. Kerjan, G. and J.G. Gleeson, *Genetic mechanisms underlying abnormal neuronal migration in classical lissencephaly.* Trends Genet, 2007. **23**(12): p. 623-30.
47. Richman, D.P., R.M. Stewart, and V.S. Caviness, Jr., *Cerebral microgyria in a 27-week fetus: an architectonic and topographic analysis.* J Neuropathol Exp Neurol, 1974. **33**(3): p. 374-84.
48. Kippenhan, J.S., et al., *Genetic contributions to human gyrification: sulcal morphometry in Williams syndrome.* J Neurosci, 2005. **25**(34): p. 7840-6.
49. Fan, C.C., et al., *Williams syndrome-specific neuroanatomical profile and its associations with behavioral features.* Neuroimage Clin, 2017. **15**: p. 343-347.
50. Van Essen, D.C., et al., *Symmetry of cortical folding abnormalities in Williams syndrome revealed by surface-based analyses.* J Neurosci, 2006. **26**(20): p. 5470-83.
51. Nordahl, C.W., et al., *Cortical folding abnormalities in autism revealed by surface-based morphometry.* J Neurosci, 2007. **27**(43): p. 11725-35.
52. Khundrakpam, B.S., et al., *Cortical Thickness Abnormalities in Autism Spectrum Disorders Through Late Childhood, Adolescence, and Adulthood: A Large-Scale MRI Study.* Cereb Cortex, 2017. **27**(3): p. 1721-1731.
53. Yang, D.Y., et al., *Cortical morphological markers in children with autism: a structural magnetic resonance imaging study of thickness, area, volume, and gyrification.* Mol Autism, 2016. **7**: p. 11.

54. Csernansky, J.G., et al., *Symmetric abnormalities in sulcal patterning in schizophrenia.* Neuroimage, 2008. **43**(3): p. 440-6.
55. Penttila, J., et al., *Cortical folding in patients with bipolar disorder or unipolar depression.* J Psychiatry Neurosci, 2009. **34**(2): p. 127-35.
56. Sarrazin, S., et al., *Neurodevelopmental subtypes of bipolar disorder are related to cortical folding patterns: An international multicenter study.* Bipolar Disord, 2018. **20**(8): p. 721-732.
57. Haldipur, P. and K.J. Millen, *What cerebellar malformations tell us about cerebellar development.* Neurosci Lett, 2019. **688**: p. 14-25.
58. Li, K., et al., *Shp2-dependent ERK signaling is essential for induction of Bergmann glia and foliation of the cerebellum.* J Neurosci, 2014. **34**(3): p. 922-31.
59. Wedeen, V.J., et al., *The geometric structure of the brain fiber pathways.* Science, 2012. **335**(6076): p. 1628-34.
60. Catani, M., I. Bodi, and F. Dell'Acqua, *Comment on "The geometric structure of the brain fiber pathways".* Science, 2012. **337**(6102): p. 1605.
61. Galinsky, V.L. and L.R. Frank, *The Lamellar Structure of the Brain Fiber Pathways.* Neural Comput, 2016. **28**(11): p. 2533-2556.
62. Economo, M.N., et al., *A platform for brain-wide imaging and reconstruction of individual neurons.* Elife, 2016. **5**: p. e10566.
63. Wang, Y., et al., *TeraVR empowers precise reconstruction of complete 3-D neuronal morphology in the whole brain.* Nat Commun, 2019. **10**(1): p. 3474.
64. Xu, F.S., Y.; Ding, L.; Yang, C-Y.; Tan, H.; Wang, H.; Zhu, Q.; Xu, R.; Wu, F.; Xu, C.; Li, Q.; Su, P.; Zhang, L.I.; Dong, H.; Desimone, R.; Xu, F.; Hu, X.; Lau, P-M.; Bi, G-Q. *High-throughput whole-brain mapping of rhesus monkey at micron resolution*. bioRxiv, 2020. DOI: 10.1101/2020.09.25.313395.
65. Van Essen, D.C., et al., *Cerebral cortical folding, parcellation, and connectivity in humans, nonhuman primates, and mice.* Proc Natl Acad Sci U S A, 2019.
66. Lewis, J.W. and D.C. Van Essen, *Mapping of architectonic subdivisions in the macaque monkey, with emphasis on parieto-occipital cortex.* J Comp Neurol, 2000. **428**(1): p. 79-111.
67. Maunsell, J.H. and D.C. Van Essen, *Topographic organization of the middle temporal visual area in the macaque monkey: representational biases and the relationship to callosal connections and myeloarchitectonic boundaries.* J Comp Neurol, 1987. **266**(4): p. 535-55.
68. Van Essen, D.C., W.T. Newsome, and J.H. Maunsell, *The visual field representation in striate cortex of the macaque monkey: asymmetries, anisotropies, and individual variability.* Vision Res, 1984. **24**(5): p. 429-48.
69. Amunts, K., et al., *Brodmann's areas 17 and 18 brought into stereotaxic space-where and how variable?* Neuroimage, 2000. **11**(1): p. 66-84.
70. Malikovic, A., et al., *Cytoarchitectonic analysis of the human extrastriate cortex in the region of V5/MT+: a probabilistic, stereotaxic map of area hOc5.* Cereb Cortex, 2007. **17**(3): p. 562-74.
71. Malikovic, A., et al., *Cytoarchitecture of the human lateral occipital cortex: mapping of two extrastriate areas hOc4la and hOc4lp.* Brain Struct Funct, 2016. **221**(4): p. 1877-97.
72. Van Essen, D.C., et al., *The projections from striate cortex (V1) to areas V2 and V3 in the macaque monkey: asymmetries, areal boundaries, and patchy connections.* J Comp Neurol, 1986. **244**(4): p. 451-80.
73. Rajimehr, R. and R.B. Tootell, *Does retinotopy influence cortical folding in primate visual cortex?* J Neurosci, 2009. **29**(36): p. 11149-52.
74. Benson, N.C., et al., *The Human Connectome Project 7 Tesla retinotopy dataset: Description and population receptive field analysis.* J Vis, 2018. **18**(13): p. 23.
75. Oh, S.W., et al., *A mesoscale connectome of the mouse brain.* Nature, 2014. **508**(7495): p. 207-14.
76. Markov, N.T., et al., *Weight consistency specifies regularities of macaque cortical networks.* Cereb Cortex, 2011. **21**(6): p. 1254-72.

77. Dehay, C., et al., *Contribution of thalamic input to the specification of cytoarchitectonic cortical fields in the primate: effects of bilateral enucleation in the fetal monkey on the boundaries, dimensions, and gyrification of striate and extrastriate cortex.* J Comp Neurol, 1996. **367**(1): p. 70-89.
78. Dehay, C., et al., *Phenotypic characterisation of respecified visual cortex subsequent to prenatal enucleation in the monkey: development of acetylcholinesterase and cytochrome oxidase patterns.* J Comp Neurol, 1996. **376**(3): p. 386-402.
79. Magrou, L., et al., *How Areal Specification Shapes the Local and Interareal Circuits in a Macaque Model of Congenital Blindness.* Cereb Cortex, 2018. **28**(8): p. 3017-3034.
80. Rakic, P., I. Suner, and R.W. Williams, *A novel cytoarchitectonic area induced experimentally within the primate visual cortex.* Proc Natl Acad Sci U S A, 1991. **88**(6): p. 2083-7.
81. Donahue, C.J., et al., *Using Diffusion Tractography to Predict Cortical Connection Strength and Distance: A Quantitative Comparison with Tracers in the Monkey.* J Neurosci, 2016. **36**(25): p. 6758-70.
82. Reveley, C., et al., *Superficial white matter fiber systems impede detection of long-range cortical connections in diffusion MR tractography.* Proc Natl Acad Sci U S A, 2015. **112**(21): p. E2820-8.
83. Jbabdi, S., et al., *Measuring macroscopic brain connections in vivo.* Nat Neurosci, 2015. **18**(11): p. 1546-55.
84. Pervaiz, U., et al., *Optimising network modelling methods for fMRI.* Neuroimage, 2020. **211**: p. 116604.
85. Smith, S.M., et al., *Functional connectomics from resting-state fMRI.* Trends Cogn Sci, 2013. **17**(12): p. 666-82.
86. Hayashi, T., Knoblauch, K., Glasser, M.F., Hou, Y., Autio, J.A., Inoue-Murayama, M., Smith, S., Kennedy, H., and Van Essen, D.C. *The NonHuman Primate Neuroimaging & Neuroanatomy Project*. 2020.
87. Lewis, J.W. and D.C. Van Essen, *Corticocortical connections of visual, sensorimotor, and multimodal processing areas in the parietal lobe of the macaque monkey.* J Comp Neurol, 2000. **428**(1): p. 112-37.
88. Autio, J.A., et al., *Towards HCP-Style macaque connectomes: 24-Channel 3T multi-array coil, MRI sequences and preprocessing.* Neuroimage, 2020. **215**: p. 116800.
89. Ali, S., et al., *Rigid and non-rigid registration of polarized light imaging data for 3D reconstruction of the temporal lobe of the human brain at micrometer resolution.* Neuroimage, 2018. **181**: p. 235-251.
90. Guo, S.M., et al., *Revealing architectural order with quantitative label-free imaging and deep learning.* Elife, 2020. **9**.
91. Striedter, G.F., S. Srinivasan, and E.S. Monuki, *Cortical folding: when, where, how, and why?* Annu Rev Neurosci, 2015. **38**: p. 291-307.
92. Borrell, V. and I. Reillo, *Emerging roles of neural stem cells in cerebral cortex development and evolution.* Dev Neurobiol, 2012. **72**(7): p. 955-71.
93. Reillo, I., et al., *A role for intermediate radial glia in the tangential expansion of the mammalian cerebral cortex.* Cereb Cortex, 2011. **21**(7): p. 1674-94.
94. Kriegstein, A., S. Noctor, and V. Martinez-Cerdeno, *Patterns of neural stem and progenitor cell division may underlie evolutionary cortical expansion.* Nat Rev Neurosci, 2006. **7**(11): p. 883-90.
95. Tallinen, T., et al., *On the growth and form of cortical convolutions.* Nature Physics, 2016. **12**(6): p. 588-593.
96. Holland, M., et al., *Symmetry Breaking in Wrinkling Patterns: Gyri Are Universally Thicker than Sulci.* Phys Rev Lett, 2018. **121**(22): p. 228002.
97. Mota, B. and S. Herculano-Houzel, *BRAIN STRUCTURE. Cortical folding scales universally with surface area and thickness, not number of neurons.* Science, 2015. **349**(6243): p. 74-7.
98. Borrell, V., *How Cells Fold the Cerebral Cortex.* J Neurosci, 2018. **38**(4): p. 776-783.
99. Ju, X.C., et al., *The hominoid-specific gene TBC1D3 promotes generation of basal neural progenitors and induces cortical folding in mice.* Elife, 2016. **5**.

100. Stahl, R., et al., *Trnp1 regulates expansion and folding of the mammalian cerebral cortex by control of radial glial fate.* Cell, 2013. **153**(3): p. 535-49.
101. Del Toro, D., et al., *Regulation of Cerebral Cortex Folding by Controlling Neuronal Migration via FLRT Adhesion Molecules.* Cell, 2017. **169**(4): p. 621-635 e16.
102. Siegenthaler, J.A., et al., *Retinoic acid from the meninges regulates cortical neuron generation.* Cell, 2009. **139**(3): p. 597-609.
103. Rash, B.G., et al., *Cortical gyrification induced by fibroblast growth factor 2 in the mouse brain.* J Neurosci, 2013. **33**(26): p. 10802-14.
104. Matsumoto, N., et al., *Gyrification of the cerebral cortex requires FGF signaling in the mammalian brain.* Elife, 2017. **6**.
105. Masuda, K., et al., *Pathophysiological analyses of cortical malformation using gyrencephalic mammals.* Sci Rep, 2015. **5**: p. 15370.
106. Haydar, T.F., et al., *The role of cell death in regulating the size and shape of the mammalian forebrain.* Cereb Cortex, 1999. **9**(6): p. 621-6.
107. Depaepe, V., et al., *Ephrin signalling controls brain size by regulating apoptosis of neural progenitors.* Nature, 2005. **435**(7046): p. 1244-50.
108. Kuida, K., et al., *Reduced apoptosis and cytochrome c-mediated caspase activation in mice lacking caspase 9.* Cell, 1998. **94**(3): p. 325-37.
109. Kuida, K., et al., *Decreased apoptosis in the brain and premature lethality in CPP32-deficient mice.* Nature, 1996. **384**(6607): p. 368-72.
110. Chenn, A. and C.A. Walsh, *Regulation of cerebral cortical size by control of cell cycle exit in neural precursors.* Science, 2002. **297**(5580): p. 365-9.
111. Kingsbury, M.A., et al., *Non-proliferative effects of lysophosphatidic acid enhance cortical growth and folding.* Nat Neurosci, 2003. **6**(12): p. 1292-9.
112. Li, Y., et al., *Induction of Expansion and Folding in Human Cerebral Organoids.* Cell Stem Cell, 2017. **20**(3): p. 385-396 e3.
113. Karzbrun, E., et al., *Human Brain Organoids on a Chip Reveal the Physics of Folding.* Nat Phys, 2018. **14**(5): p. 515-522.
114. Bayly, P.V. and J.R. Garbow, *Pre-clinical MR elastography: Principles, techniques, and applications.* J Magn Reson, 2018. **291**: p. 73-83.
115. Chatelin, S., et al., *An automatic differentiation-based gradient method for inversion of the shear wave equation in magnetic resonance elastography: specific application in fibrous soft tissues.* Phys Med Biol, 2016. **61**(13): p. 5000-19.
116. Guertler, C.A., et al., *Estimation of Anisotropic Material Properties of Soft Tissue by Mri of Ultrasound-induced Shear Waves.* J Biomech Eng, 2020.
117. Smith, D., et al., *Multi-Excitation MR Elastography of the Brain: Wave Propagation in Anisotropic White Matter.* J Biomech Eng, 2020.
118. Van Essen, D.C., *A tension-based theory of morphogenesis and compact wiring in the central nervous system.* Nature, 1997. **385**(6614): p. 313-8.
119. Bringmann, A., et al., *The primate fovea: Structure, function and development.* Prog Retin Eye Res, 2018. **66**: p. 49-84.
120. Kirby, M.A. and T.C. Steineke, *Morphogenesis of retinal ganglion cells during formation of the fovea in the Rhesus macaque.* Vis Neurosci, 1992. **9**(6): p. 603-16.
121. Steineke, T.C. and M.A. Kirby, *Early axon outgrowth of retinal ganglion cells in the fetal rhesus macaque.* Brain Res Dev Brain Res, 1993. **74**(2): p. 151-62.
122. Springer, A.D. and A.E. Hendrickson, *Development of the primate area of high acuity. 1. Use of finite element analysis models to identify mechanical variables affecting pit formation.* Vis Neurosci, 2004. **21**(1): p. 53-62.
123. Springer, A.D. and A.E. Hendrickson, *Development of the primate area of high acuity, 3: temporal relationships between pit formation, retinal elongation and cone packing.* Vis Neurosci, 2005. **22**(2): p. 171-85.
124. Kelling, S.T., et al., *Differential elasticity of the immature retina: a contribution to the development of the area centralis?* Vis Neurosci, 1989. **2**(2): p. 117-20.
125. Kuhrt, H., et al., *Postnatal mammalian retinal development: quantitative data and general rules.* Prog Retin Eye Res, 2012. **31**(6): p. 605-21.

126. Cornish, E.E., et al., *Gradients of cone differentiation and FGF expression during development of the foveal depression in macaque retina.* Vis Neurosci, 2005. **22**(4): p. 447-59.
127. Cornish, E.E., et al., *Differential distribution of fibroblast growth factor receptors (FGFRs) on foveal cones: FGFR-4 is an early marker of cone photoreceptors.* Mol Vis, 2004. **10**: p. 1-14.
128. Provis, J.M., et al., *Adaptation of the central retina for high acuity vision: cones, the fovea and the avascular zone.* Prog Retin Eye Res, 2013. **35**: p. 63-81.
129. Goldberg, A.F., O.L. Moritz, and D.S. Williams, *Molecular basis for photoreceptor outer segment architecture.* Prog Retin Eye Res, 2016. **55**: p. 52-81.
130. Witter, M.P., *The perforant path: projections from the entorhinal cortex to the dentate gyrus.* Prog Brain Res, 2007. **163**: p. 43-61.
131. Deng, J.B., et al., *The tracing study of developing entorhino-hippocampal pathway.* Int J Dev Neurosci, 2007. **25**(4): p. 251-8.
132. Tamamaki, N., *Development of afferent fiber lamination in the infrapyramidal blade of the rat dentate gyrus.* J Comp Neurol, 1999. **411**(2): p. 257-66.